International Journal of Refrigeration 159 (2024) 50–63

Contents lists available at ScienceDirect

International Journal of Refrigeration

journal homepage: www.elsevier.com/locate/ijrefrig

# Advanced exergy analysis of a Reverse Brayton cycle using air as working fluid for cryogenic purposes

## *Analyse exergétique avancée d'un cycle de Brayton inversé utilisant l'air comme fluide de travail à des fins cryogéniques*

José Ramón Serrano, Vicente Dolz, Alejandro Gómez-Vilanova *, Juan Antonio López-Carrillo

*CMT – Motores Térmicos, Universitat Politècnica de València, Spain*

ARTICLE INFO

*Keywords:*
Exergy analysis
Reverse Brayton cycle
Air-based cycles
Radial turbine
Turbocharger

*Mots clés:*
Analyze exergétique
Cycle de Brayton inverse
Cycles à air
Turbine radiale
Turbocompresseur

ABSTRACT

The global push to reduce greenhouse gas emissions has led to the ban of high global warming potential (GWP) refrigerants in the refrigeration sector, prompting the adoption of low-GWP alternatives. However, as regulations are expected to tighten, technologies like the Reverse Brayton cycles (RBC) are emerging. RBCs can operate with safe fluids and can reach very low temperatures through compressions, regeneration, and expansion, requiring only electricity. This research presents results from an RBC equipped with a radial turbine using natural air (R-729), a hazard-free fluid with zero ozone depletion potential (ODP) and emission potential. The cycle utilizes automotive components, offering a cost-effective, high-tech solution. The study evaluates the cycle COP at a design point and performs an exergetic analysis at 173K. Using a thermal and fluid dynamic model of the cycle, the critical components of the cycle influencing the COP are identified, and potential improvements are explored.

## 1. Introduction

Refrigeration services play a significant role in the contemporary world and its economy. It is crucial for a range of sectors, such as food, health, energy, or air-conditioning. Ensure cold chain transportation conditions became a global concern during the COVID-19 pandemic when a vaccine was developed. The necessity of transporting billions of doses all over the world with temperatures as low as −90 °C (World Health Organization et al., 2021) without breaking the cold chain to avoid degradation was a challenge to face. Several technologies were combined to achieve the goal of vaccine transportation, combining different approaches (Pambudi et al., 2022) and requiring various levels of qualification in the people involved in the process. Different regions have different regulations on refrigerants permitted or banned since by May 2023, just 148 countries have accepted and applied (ratified or provisionally) the Kigali Amendment (United Nations Environment Program, 2023). This international agreement looks for a phase-down in current refrigerant fluids based on hydrofluorocarbons (HFCs), with a projected cut of over 60% HFC emissions by 2050 (Höglund-Isaksson et al., 2017). The expected reduction in emissions turns into a remarkable number, considering the estimated impact of HFC on world total greenhouse gases (GHG) emissions being 7.8% (Dupont et al., 2019).

Thus, the evolution into low-GWP refrigerants is underway. This is considered the 4th generation of refrigerants (Shuailing et al., 2022) since the first steps of refrigeration technology during the 19th century. This generational change, motivated by the need to reduce global warming effects, started in the decade of 2010s and has faced different problems. Flammability, pressure needs, toxicity, market availability, and production cost while still having considerable values for GWP (in the order of tens or hundreds) (Yana Motta and Domanski, 2022) showed a way for natural refrigerants. Ammonia and Carbon dioxide are the main candidates to take the market in large commercial and industrial applications for refrigeration. Even though, Nitrogen and air are also considered aspirants for refrigeration in the upcoming years. Food freezing (Biglia et al., 2017), (Biglia et al., 2022); refrigerated transport (Spence et al., 2004, 2005); whole and partial-body cryotherapy (Dugue et al., 2020) appear as sectors in which these fluids can make an impact. By targeting air as refrigerant, multiple benefits can be achieved. First, its availability can be considered endless and free-cost; it is safe since it is obviously hazardless for humans and not flammable. There is no pollution generation because of the fluid itself. Leakages in the system do not drive into high-cost refills of the system.

* Corresponding author.
*E-mail address:* alejandro.gomez.vilanova.upv@gmail.com (A. Gómez-Vilanova).

https://doi.org/10.1016/j.ijrefrig.2023.12.002
Received 19 June 2023; Received in revised form 3 November 2023; Accepted 2 December 2023
Available online 5 December 2023

**Nomenclature**

**Subscripts & superscripts**

| | |
|---|---|
| 0 | Total conditions |
| a | Air |
| AV | Avoidable |
| CC | Climatic Chamber |
| CH | Chemical |
| D | Destruction |
| EC | Electric Compressor |
| EN | Endogenous |
| EX | Exogenous |
| F | Fuel |
| IC | Inter-Cooler |
| in | Inlet side |
| k | $k$th component |
| KIN | Kinetic |
| L | Losses |
| M | Mechanical |
| out | Outlet side |
| P | Product |
| PH | Physical |
| POT | Potential |
| RBC | Reverse Brayton Cycle |
| Reg | Regenerator |
| T | Thermal |
| TCC | Turbocharger Compressor |
| TL | Thermal load |
| tot | Total |
| Turb | Turbine |
| UN | Unavoidable |
| w | Water |

**Symbols**

| | |
|---|---|
| $\dot{E}$ | Exergy |
| $\dot{m}$ | Mass Flow Rate [kg/s] |
| $\dot{Q}$ | Heat |
| $\dot{W}$ | Work |
| $\epsilon$ | Exergetic Efficiency |
| $\eta$ | Corresponding Efficiency |
| $c_p$ | Specific Heat at Constant Pressure [J/kg/K] |
| CC | Climatic Chamber |
| COP | Coefficient of Performance [-] |
| e | Specific Exergy |
| EC | Electric Compressor |
| FOM | Figure of Merit |
| GHG | Greenhouse gases |
| GWP | Global Warming Potential |
| h | Enthalpy |
| IC | Inter-Cooler |
| MFR | Mass Flow Rate [kg/s] |
| ODP | Ozone Depletion Potential |
| P | Pressure [bar] |
| R | Gas constant |
| RBC | Reverse Brayton Cycle |
| Reg | Regenerator |
| s | Entropy |
| T | Temperature [°C] |
| TCC | Turbocharger Compressor |
| Turb | Turbine |
| Unav | Unavoidable |
| VGT | Variable Geometry Turbine |
| y | Exergy Destruction Ratio |

The achievable temperature range goes from the ambient level to the Nitrogen boiling point (−195.8 °C). Maximum pressure levels can be kept at the operating range of conventional turbochargers, below 5 bars, which means the system operation is safe and maintenance costs can be reduced. Furthermore, in contrast with the exigence of the aforementioned systems of cold chain transportation for vaccines, there is no need for a high qualification to operate a facility working with air as a refrigerant fluid.

Reverse Brayton cycles have been proven to be an interesting option for refrigeration purposes, as stated in the review of this topic from Shuailing et al. (2022). Besides, other recent contributions to the topic can be found in Serrano et al. (2022) and Yang et al. (2023), using turboexpanders attached to centrifugal compressors to make use of the work output produced in the turbine during the expansion process. The systems showed good behavior when it came to dissipating a few kilowatts with COP values from around 0.1 at temperatures below −100 °C (Serrano et al., 2022) to nearly one at ambient temperature (Yang et al., 2023). The turbine isentropic efficiency seems to be the key factor in improving COP, especially in the case of regenerative RBC. However, in the available literature, there is a lack of information regarding exergy analysis for these kinds of cycles working with air, specially in the cryogenic-temperature range. Some authors as Lu et al. (2023) studied different configurations of Brayton cycles for refrigeration purposes analyzing the exergy loss under a conventional analysis but for wastewater treatment in a range over 60 °C. This reinforces the flexibility this kind of cycles have in the range of temperatures they can work at. Wang et al. (2023) also studied a RBC for air conditioning, they proposed a novel centrifugal cycle using a rotating heat-exchanger and evaluated air as one of the potential fluids for the purpose. Sun et al. (2023) made computational work studying RBC in the range of −60 °C to −120 °C but using refrigerant fluids instead of air.

Exergy analysis discerns the origins, scale, and positioning of thermodynamic inefficiencies within a system, guiding enhancements by highlighting elements with pronounced exergy imbalances. Yet, conventional exergy analysis assesses component performance in isolation, neglecting interactions among components. Advanced exergy analysis (Morosuk et al., 2013) rectifies this by partitioning exergy into endogenous/exogenous and avoidable/unavoidable categories. Parsing exergy into avoidable and unavoidable measures the efficiency improvement potential of a component, while the endogenous and exogenous split illustrates interactions between system components. In Dhillon and Ghosh (2021), a contribution to the understanding of the exergy behavior of various configurations of RBC for cryogenic purposes is done, but using liquid Nitrogen as working fluid. Other studies on RBC evaluate their economic analysis (Huang et al., 2022), but in this case, for a $CO_2$ cycle. In refrigeration systems, in general, numerous exergy analyses have been performed in recent years, as for example, Chen et al. (2015), who analyzed an ejector refrigeration system, as well as Galindo et al. (2020), doing an advanced exergy analysis for another jet ejector refrigeration cycle. Other authors as Asgari et al. (2017), optimized an internal auto-cascade refrigeration cycle. Galindo et al. (2016) proposed an advanced exergy analysis for a bottoming organic Rankine cycle in combination with an internal combustion engine. Hu et al. (2020), did an exergy analysis on a Brayton cycle, focusing on the study of different cooling modes. Entering in the low-GWP refrigerants, Qin et al. (2021), performed an energy and exergy

study on auto-cascade refrigeration systems for temperatures down to −100 °C. Khalilzadeh et al. (2023), have shown a comparison between different thermodynamic cycles as an Organic Rankine and a Kalina cycle through exergy analysis attending to refrigeration demands. Still, as previously stated, no single one has been found for the application of an RBC using air as the working fluid. Furthermore, advanced exergy analysis is planned for this purpose since it provides information on potential improvement for each component and the whole cycle and shows the interaction between components.

Since the RBC can target multiple objectives, a fixed point for dissipating 1.5 kW in a climatic chamber at −100 °C is chosen to be tested on an experimental facility. This point covers the need for a whole-body cryotherapy cabin with a person inside for the recommended period of 3 min (Dugue et al., 2020), or the storage of an equivalent load of frozen product for an undefined period of time. The advantage of the system, besides the benefits of the air, is that an electric power source runs it. Electric motors drive two centrifugal compressors. Thus, the system makes it possible to be fueled by batteries and fully portable. This would allow an unstopped cold chain storage for any frozen freight that needs to be transported. No environmental regulation is applied to the system anywhere in the world because of its null ODP and ultra-low GWP. The objective of the paper is to identify, through an exergy analysis, the key components in an RBC to improve the COP of the system. To do so, an experimental facility is developed and described as shown in Section 2. After that, a thermodynamic analysis of the cycle is depicted in Section 3, showing the approach that will be followed in Section 4 where, after the validation of experimental results through a 1D model, prospective studies and advanced analyses are performed. Finally, with the exergy analysis of every studied case, it will be identified how an experimental facility can be improved as well as its potential expected maximum COP for a design point.

The originality of this study is that it presents potential improvements in air-based refrigeration cycles based on actual experimental data. These experimental results are obtained from a testing facility built with commercial components that have not been specifically designed for this type of application but are easy to acquire and have a low cost, high reliability, and easy maintenance.

## 2. Description of the RBC

The developed facility for testing the assembled automotive components is shown in Figs. 1 and 2, while the schematic diagram of the proposed cycle is shown in Fig. 3. The two electric compressors (Rotrex® models EC15-60 and EC15-20 respectively) are responsible for providing mechanical exergy to the system due to the increment in pressure levels that they provoke in the successive compression stages (between stages 1–2 and 3–4 for the electric compressors and stages 4–5 for the TCC). Heat exchangers are air-to-water coolers, compact in size and fed by a water supply at ambient temperature (components from Valeo® model 818727). They are placed between the two electric compressors (stages 2–3) and after the turbocharger compressor (stages 5–6), which enhances pressure by taking advantage of the power generated by the turbine (manufactured by BorgWarner® model BV38). The regenerator is an air-to-air heat exchanger from Alfa Laval® (model AlfaNova HP 76-100H) where high-pressure fluid switches temperature with a lower-pressure (and lower-temperature) fluid that has been expanded in the radial turbine (stages 7–8). This closed loop allows reaching cryogenic temperatures that find their limit in the overall power of the system and the regenerator efficiency. The turbine is equipped with a variable nozzle vanes system. After the expansion, the air passes through a centrifugal cyclonic separator that collects the humidity of fresh air when it reaches the dew point, and any possible lube-oil drop leak from any of the rotatory machines. The heat dissipated in the climatic chamber depends on the thermal load applied (stages 8–9).

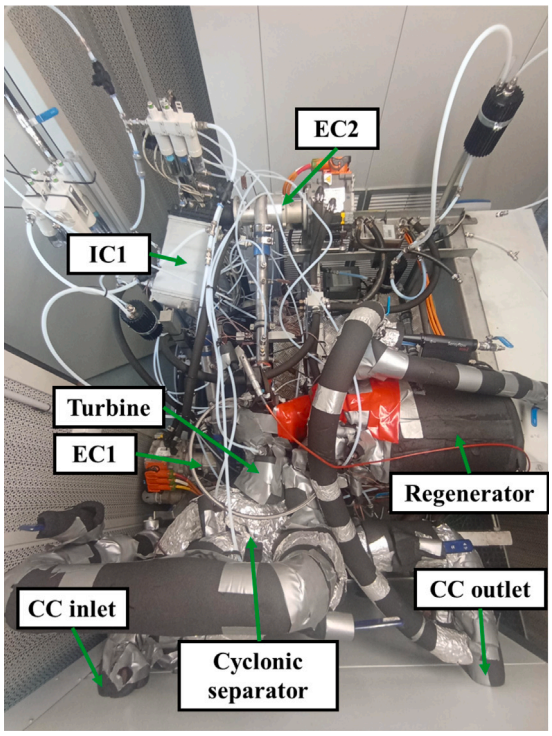


**Fig. 1.** Reverse Brayton Cycle test rig. Top view.

Once the minimum cycle temperature has been achieved, it is delivered to the climatic chamber to refrigerate the thermal load, simulated by an electrical heater. This interaction can occur either in an open or closed cycle. In the open cycle, the air gets in contact with the product to refrigerate it mainly by forced convection. The other option is a closed cycle where the air passes through a heat exchanger, so the cooling process is through radiation and natural convection mainly.

Both thermocouples and pressure sensors have been placed upstream and downstream of each element in the cycle to capture its performance and get information to diagnose and build a thermal and fluid dynamic model of the test rig. This task would ease a first approach to new cycle configurations or the use of new components. The characteristics of the transducers used during the experimental research in the reverse Brayton cycle were:

- Mass flow rate: It is important to highlight that while mass flow meters from a turbocharger gas stand were used to measure the turbocharger mass flows, they were not utilized directly in the reverse Brayton cycle facility. However, the turbomachinery adiabatic maps obtained from the gas stand acted as transducers to gauge the mass flow in the reverse Brayton cycle. They were measured at both inlet and outlet of turbine and compressor with hot-film and vortex mass flow meters. These were calibrated for air, allowing a maximum flow rate of 0.200 kg/s. The uncertainty of the devices had a uniform distribution for measurements over 0.005 kg/s of 1.1% from the measured value, and the imbalance between the inlet and outlet was checked. Results and information about the turbocharger test rig used to characterize the component are shown in Serrano et al. (2021).
- Temperature: Three T-type thermocouples were placed upstream and downstream of each element. They were placed radially distributed at the same diameter with 120 ° between them and

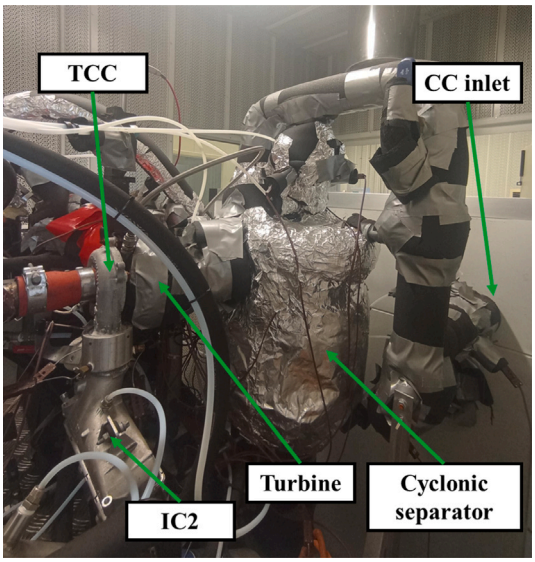


**Fig. 2.** Reverse Brayton Cycle test rig. Side view.

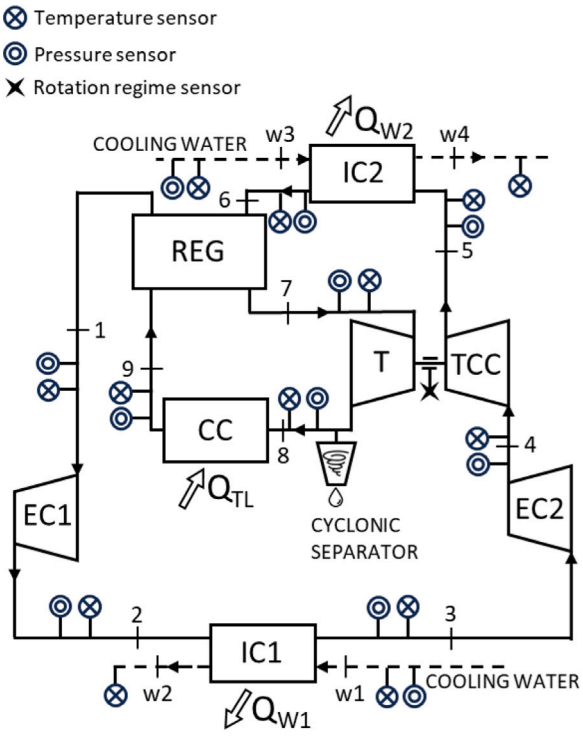


**Fig. 3.** Reverse Brayton Cycle diagram.

inserted at different depths. Their uncertainty was 0.5 K. To reduce the propagated uncertainty, each channel in the acquisition system was individually calibrated.

- Pressure: Absolute pressure piezoresistive transducers were employed at each cycle stage. They were placed upstream of the thermocouples to avoid distortion in measurements. Their measure range varied between 0 – 2.5 bar to 0 – 6 bar, and the uncertainty had a non-linearity of 0.5%.

## 3. Thermodynamic analysis

The diagram shown in Fig. 3 includes the main components of the cycle, turbine and compressors, coolers, a regenerator, and the chamber where the thermal load is kept. Cooling water through the coolers is considered in the analysis, and power is applied to the thermal load.

Based on the following assumptions, the results of a model of the cycle are exergetically analyzed.

- Air in the cycle is considered dried with no humidity.
- System works under steady-state conditions.
- Pressure and heat losses in the pipes are neglected since they have been thermally insulated, and cross sections are designed to keep the air at low velocities inside (< 40 m/s)
- Kinetic exergy is negligible.
- The potential exergy is consistent across the entry and exit points of each component. Therefore it can be neglected.
- The RBC does not count with any chemical reaction, so chemical exergy is zero.
- Reference conditions for both temperature and pressure for every studied case are set as $T_0 = 25$ °C and $P_0 = 101325$ Pa
- The climatic chamber pressure is ambient for every studied case.
- Target temperature in the CC is −100 °C and the thermal load dissipated is 1.5 kW.

For the thermodynamic evaluation of the cycle display, it is used a figure of merit (Eq. (3)) based on the formulation of Dhillon and Ghosh (2021) using a ratio between the actual coefficient of performance (COP) and the ideal one, which lays on the definition from Timmerhaus and Flynn (2013). COP is the ratio of the refrigeration capacity in the climatic chamber to the input energy required, in this case, in the form of enthalpy change in the electric compressors. Actual and ideal COP values are defined as shown in Eqs. (1) and (2).

$$COP_{actual} = \frac{\left(T_{out,CC} - T_{in,CC}\right)}{\left(T_{out,EC1} - T_{in,EC1}\right) + \left(T_{out,EC2} - T_{in,EC2}\right)} \tag{1}$$

$$COP_{ideal} = \frac{\left(T_{out,CC} - T_{in,CC}\right)}{T_w \ln T_{out,CC}/T_{in,CC} - \left(T_{out,CC} - T_{in,CC}\right)} \tag{2}$$

$$FOM = \frac{COP_{actual}}{COP_{ideal}} \tag{3}$$

In the different COP formulations, the temperatures refer to the air at the corresponding component, but for $T_w$ that is the water temperature, which is the minimum temperature that can be achieved prior to the regeneration stage.

### 3.1. Conventional exergy analysis

Exergy measures the maximum theoretical work that can be extracted from a thermodynamic system. It can be measured as the deviation between the conditions at each system stage and the reference state. Through the exergy analysis of the thermodynamic cycle defined in this work, it will be possible to identify the sources of inefficiency and to determine the potential for improvement in the referred system. The total exergy in a system is the sum of physical, chemical, kinetic, and potential exergy, as expressed in Eq. (4).

$$\dot{E} = \dot{E}^{PH} + \dot{E}^{CH} + \dot{E}^{KIN} + \dot{E}^{POT} \tag{4}$$

As declared on the assumptions for this calculation, chemical, kinetic and potential exergy can be neglected. Thus, only physical exergy is considered for the analysis; this involves both thermal ($\dot{E}^T$ due to temperature deviation with the environment) and mechanical ($\dot{E}^M$ mostly due to pressure variation with respect to ambient one) exergy, related as shown in Eq. (5).

$$\dot{E}^{PH} = \dot{E}^T + \dot{E}^M = \dot{m}e^T + \dot{m}e^M \tag{5}$$

Where $e$ is the specific exergy and for each analyzed station of the system can be obtained as in Eq. (6).

$$\begin{aligned} e &= (h-h_0) - T_0(s-s_0) \\ &= [(h-h_X) - T_0(s-s_X)]_{p=const} \\ &+ [(h_X-h_0) - T_0(s_X-s_0)]_{T_0=const} \\ &= e^T + e^M \end{aligned} \tag{6}$$

Being $X$ the point defined with the pressure of the corresponding station and reference temperature.

As previously stated, being air considered as dried, both enthalpy and entropy are obtained from the Open-Source Thermophysical Property Library CoolProp (Bell et al., 2014).

The thermodynamic cycle method to analyze the exergy using the concepts of fuel and product for each component is detailed now. To determine the irreversibility of the system, the notion of exergy destruction comes out as the portion that lies between exergy fuel, total input at each element, and exergy product, the one finally obtained. The relation between the three contenders can be seen in Eq. (7).

$$\dot{E}_{F,k} = \dot{E}_{P,k} + \dot{E}_{D,k} \tag{7}$$

Where the subscript $k$ stands for the $k$th component being analyzed (turbine, compressors, coolers, regenerator, and climatic chamber).

The term $\dot{E}_F$ is the exergy of fuel, not an actual fuel but the exergy supply applied on a component to obtain the desired $\dot{E}_P$, or exergy of product, with the loss of exergy represented by $\dot{E}_{D,k}$ for each $k$ component. However, when the exergy of the whole system is considered at once, a new term of losses should be taken into account. According to Petrakopoulou et al. (2011) and Bakshi et al. (2011), assuming that the system boundaries for exergy balance calculations in each component are at the temperature $T_0$, no exergy losses are being attributed to any specific component by this matter (irreversibilities only come from exergy destruction at each $k$th component), so a new term $\dot{E}_{L,tot}$ appears at the level of the overall system, representing the external exergy loss in the system. The exergy balance is as in Eq. (8).

$$\dot{E}_{F,tot} = \dot{E}_{P,tot} + \sum_{k=1}^{n} \dot{E}_{D,k} + \dot{E}_{L,tot} \tag{8}$$

In the conventional exergy analysis, two dimensionless variables are used for each $k$th component of the system, the exergetic efficiency and the exergy-destruction ratio. The exergetic efficiency can be evaluated for each component and the whole system, being the ratio between the exergy of product and fuel. it is expressed as $\epsilon$ and the equations that define both efficiencies are shown in Eqs. (9) and (10).

$$\epsilon_k = \frac{\dot{E}_{P,k}}{\dot{E}_{F,k}} = 1 - \frac{\dot{E}_{D,k}}{\dot{E}_{F,k}} \tag{9}$$

$$\epsilon_{tot} = \frac{\dot{E}_{P,tot}}{\dot{E}_{F,tot}} = 1 - \sum_{k=1}^{n} y_k - \frac{\dot{E}_{L,tot}}{\dot{E}_{F,tot}} \tag{10}$$

Being $y_k$ the other dimensionless variable aforementioned, which is the exergy-destruction ratio. Defined as the fraction between the destruction exergy of a $k$th component and the total fuel exergy of the system. Complementary, $y_k^*$ is the percentual contribution of each component to the total destruction exergy in the system. The expressions for these definitions are shown in Eqs. (11) and (12).

$$y_k = \frac{\dot{E}_{D,k}}{\dot{E}_{F,k}} \tag{11}$$

$$y_k^* = \frac{\dot{E}_{D,k}}{\dot{E}_{D,tot}} \tag{12}$$

The exergy balance for each element in the cycle has been calculated according to the equations from Table 1.

### 3.2. Advanced exergy analysis

Advanced exergy analysis is recommended for further detailed analysis of how each component affects the exergy of the system and to get to know the connections between them. To do so, exergy is split into endogenous/exogenous and avoidable/unavoidable.

### 3.3. Endogenous/exogenous

Exergy destruction in a $k$th component does not usually depend exclusively on itself so it can be divided into endogenous and exogenous exergy destruction. Endogenous ($\dot{E}_{D,k}^{EN}$) is the name of the exergy destruction that takes place on a hybrid cycle where the $k$th element operates in real conditions while all of the other components of the system act under ideal conditions. Exogenous exergy destruction ($\dot{E}_{D,k}^{EX}$) is the difference between the exergy destruction from the conventional analysis and the endogenous exergy destruction, as shown in Eq. (13).

$$\dot{E}_{D,k} = \dot{E}_{D,k}^{EN} + \dot{E}_{D,k}^{EX} \tag{13}$$

This implies that other components partly cause the destruction of exergy in that $k$th element. Observing both endogenous and exogenous exergy destruction is beneficial to the analysis since it helps assess whether the focus should be directed towards the $k$th component or another one for optimization.

### 3.4. Avoidable/unavoidable

On the other hand, exergy destruction on a $k$th component of the system can be divided into avoidable ($\dot{E}_{D,k}^{AV}$) and unavoidable ($\dot{E}_{D,k}^{UN}$), being the avoidable part the one that could be suppressed if the component is improved up to its technical limits, either by technology, materials, manufacturing methods or any other way to improve the component. Unavoidable exergy destruction is, as its name indicates, the part that is inherent to implementing the component on the system and cannot be surpassed, as shown in Eq. (14).

$$\dot{E}_{D,k} = \dot{E}_{D,k}^{AV} + \dot{E}_{D,k}^{UN} \tag{14}$$

Where $\dot{E}_{D,k}^{UN}$ is defined as the product exergy of a $k$th component multiplied by the ratio of exergy destruction and product exergy of that $k$th element under unavoidable conditions, as shown in Eq. (15).

$$\dot{E}_{D,k}^{UN} = \dot{E}_{P,k} \left( \frac{\dot{E}_D}{\dot{E}_P} \right)_k^{UN} \tag{15}$$

And $\dot{E}_{D,k}^{AV}$ is directly the difference of $\dot{E}_{D,k}^{UN}$ and the total destruction exergy (Eq. (16)).

$$\dot{E}_{D,k}^{AV} = \dot{E}_{D,k} - \dot{E}_{D,k}^{UN} \tag{16}$$

### 3.5. Combination of both splitting approaches

The two approaches to perform an advanced exergy analysis shown in this work can be combined to obtain Eq. (17).

$$\dot{E}_{D,k} = \dot{E}_{D,k}^{EN,AV} + \dot{E}_{D,k}^{EN,UN} + \dot{E}_{D,k}^{EX,AV} + \dot{E}_{D,k}^{EX,UN} \tag{17}$$

The terms from Eq. (17) can be explained as $\dot{E}_{D,k}^{EN,AV}$ being the exergy destruction that is avoidable by increasing the efficiency on the $k$th component up to its technological limits (Eq. (20)); $\dot{E}_{D,k}^{EN,UN}$ is the minimum exergy destruction that the $k$th element will suffer no matter what modifications are applied at the cycle. It is caused by itself and cannot be recovered or reduced, and it is obtained as Eq. (18). By its part, $\dot{E}_{D,k}^{EX,AV}$ is the controllable part of exergy destruction for the $k$th component improving the other components of the system, and is calculated as shown in Eq. (21). Finally, $\dot{E}_{D,k}^{EX,UN}$ stands for the exergy

**Table 1**
Exergy balance equations.

| | Fuel Exergy $\dot{E}_{F,k}$ | Product Exergy $\dot{E}_{P,k}$ | Destruction Exergy $\dot{E}_{D,k}$ |
|---|---|---|---|
| EC1 | $\dot{E}_{F,EC1} = \dot{W}_{EC1}$ | $\dot{E}_{P,EC1} = \dot{m}_a(e_2 - e_1)$ | $\dot{E}_{D,EC1} = \dot{E}_{F,EC1} - \dot{E}_{P,EC1}$ |
| IC1 | $\dot{E}_{F,IC1} = \dot{m}_a(e_2 - e_3)$ | $\dot{E}_{P,IC1} = \dot{m}_w(e_{w2} - e_{w1})$ | $\dot{E}_{D,IC1} = \dot{E}_{F,IC1} - \dot{E}_{P,IC1}$ |
| EC2 | $\dot{E}_{F,EC2} = \dot{W}_{EC2}$ | $\dot{E}_{P,EC2} = \dot{m}_a(e_4 - e_3)$ | $\dot{E}_{D,EC2} = \dot{E}_{F,EC2} - \dot{E}_{P,EC2}$ |
| TCC | $\dot{E}_{F,TCC} = \dot{W}_{TCC}$ | $\dot{E}_{P,TCC} = \dot{m}_a(e_5 - e_4)$ | $\dot{E}_{D,TCC} = \dot{E}_{F,TCC} - \dot{E}_{P,TCC}$ |
| IC2 | $\dot{E}_{F,IC2} = \dot{m}_a(e_5 - e_6)$ | $\dot{E}_{P,IC2} = \dot{m}_w(e_{w4} - e_{w3})$ | $\dot{E}_{D,IC2} = \dot{E}_{F,IC2} - \dot{E}_{P,IC2}$ |
| Reg | $\dot{E}_{F,Reg} = \dot{m}_a(e_6 - e_7)$ | $\dot{E}_{P,Reg} = \dot{m}_a(e_1 - e_9)$ | $\dot{E}_{D,Reg} = \dot{E}_{F,Reg} - \dot{E}_{P,Reg}$ |
| Turb | $\dot{E}_{F,Turb} = \dot{m}_a(e_7^M - e_8^M)$ | $\dot{E}_{P,Turb} = \dot{m}_a(e_8^T - e_7^T) + \dot{W}_{Turb}$ | $\dot{E}_{D,Turb} = \dot{E}_{F,Turb} - \dot{E}_{P,Turb}$ |
| CC | $\dot{E}_{F,CC} = \dot{Q}_{TL}$ | $\dot{E}_{P,CC} = \dot{m}_a(e_9 - e_8)$ | $\dot{E}_{D,CC} = \dot{E}_{F,CC} - \dot{E}_{P,CC}$ |
| Cycle | $\dot{E}_{F,tot} = \dot{E}_{F,EC1} + \dot{E}_{F,EC2}$ | $\dot{E}_{P,tot} = \dot{E}_{P,CC}$ | $\dot{E}_{D,tot} = \sum \dot{E}_{D,k}$ |

destruction that cannot be eliminated for technical barriers in the other components of the cycle, obtained as in Eq. (19).

$$\dot{E}_{D,k}^{UN,EN} = \dot{E}_{P,k}^{EN}\left(\frac{\dot{E}_D}{\dot{E}_P}\right)_k^{UN} \tag{18}$$

$$\dot{E}_{D,k}^{UN,EX} = \dot{E}_{D,k}^{UN} - \dot{E}_{D,k}^{UN,EN} \tag{19}$$

$$\dot{E}_{D,k}^{AV,EN} = \dot{E}_{D,k}^{EN} - \dot{E}_{D,k}^{UN,EN} \tag{20}$$

$$\dot{E}_{D,k}^{AV,EX} = \dot{E}_{D,k}^{EX} - \dot{E}_{D,k}^{UN,EX} \tag{21}$$

## 4. Results and discussion

To perform the whole exergy analysis, a 1D simulation model is employed. The models employed in this study are constructed and embedded into Virtual Engine Model (VEMOD), an in-house and non-commercial gas-dynamic software that researchers have developed at CMT-Clean Mobility & Thermofluids (Martin et al., 2018). Firstly, the model is validated against experimental data to check its reliability. The turbocharger employed was the same as in Serrano et al. (2021), where the effectiveness of the extrapolation model for the turbine was tested. The whole turbocharger model is explained in different articles as in Serrano et al. (2016, 2019b,a). From the vast testing campaign carried out with the facility, whose results are shown in Serrano et al. (2022), a new map for the turbine is built to avoid the differences observed between adiabatic and cryogenic measurements. The same under cryogenic conditions measured points are used to build the map for the TCC. The manufacturer provides maps from the two electric compressors, but those maps have been corrected according to the actual experimental results since some areas of the map were mispredicted. For the regenerator, a correlation was provided by the manufacturer to obtain efficiency according to the MFR. Its validity was checked, and the pressure loss was adapted to the different testing conditions. The two inter-coolers were modeled using a correlation dependent on the water mass flow and inlet temperature and on the inlet pressure and temperature leap in the air side of the inter-coolers.

In Figs. 4 and 5, figures for the accordance between experimental and model results are developed. The working point selected is, as previously exposed, one targeting to dissipate 1.5 kW in the CC while maintaining it at a temperature of −100 °C and ambient pressure. Both electric compressor rotational speeds were chosen to be close to their optimum efficiency map area, and the VGT was set in the peak turbine isentropic efficiency performance, according to the testing campaign from Serrano et al. (2022). Fig. 4 represents the evolution of temperature (in Kelvin degree) for every stage of the cycle, while Fig. 5 does the same for pressure (in bar). Numbers in the vertices of the polygon stand for the stages in the cycle according to the numeration in Fig. 3. On the temperature side, there have been pointed out both the target temperature in the CC, achieved in point 9, and the water cooling line temperature, being 3 and 6, the points that should be closer to that value. On the pressure plot, an additional line indicates ambient

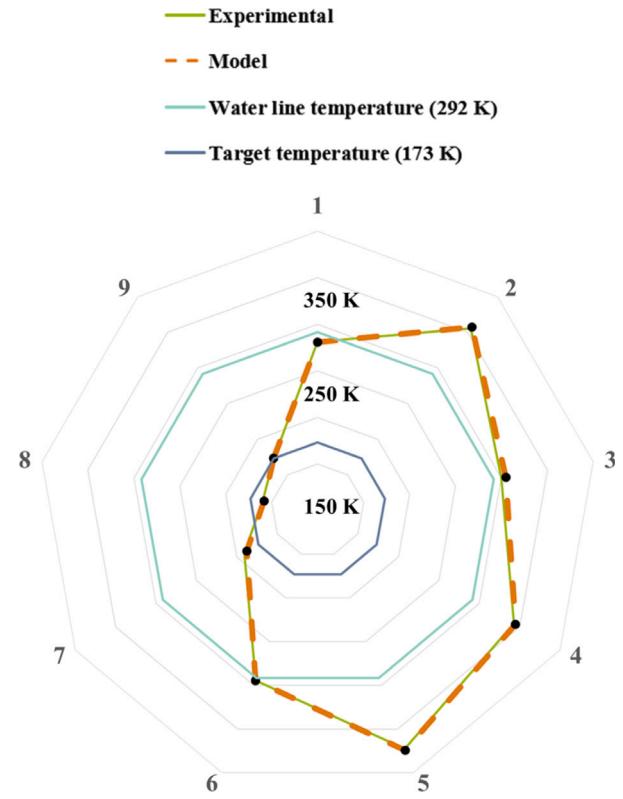


**Fig. 4.** Validation of temperature in the cycle.

pressure, the one reached at point 9. By looking at Fig. 4, the agreement between the experimental (green solid line) and model results (orange dotted line) is within the range of ±4 °C. The highest difference is on point 3 (IC1 outlet), overpredicting the model by 4 °C. The extensive amount of experimental points for adjusting the model allowed to fit the pressure losses in the facility for a wide range of MFR, and as a result of it, in Fig. 5, the maximum error is within $\pm 80 mbar$. Maximum pressure reaches 3 bar, and the minimum temperature in the cycle (turbine outlet) is −112.5 °C for the experiment, and −114.8 °C for the model.

Once the model is validated, some simplifications will be applied. The pipes in the facility were placed to allow flow development before sensors (6 diameters after discontinuities and one diameter between pressure and temperature sensors in the same station) and to adapt the facility to the laboratory environment. The number of sensors is oversized for experimental purposes so that it can be highly reduced, and therefore piping can be shortened and optimized for further pressure loss reduction. Considering this, a second simulation with the components modeled according to their experimental behavior but with

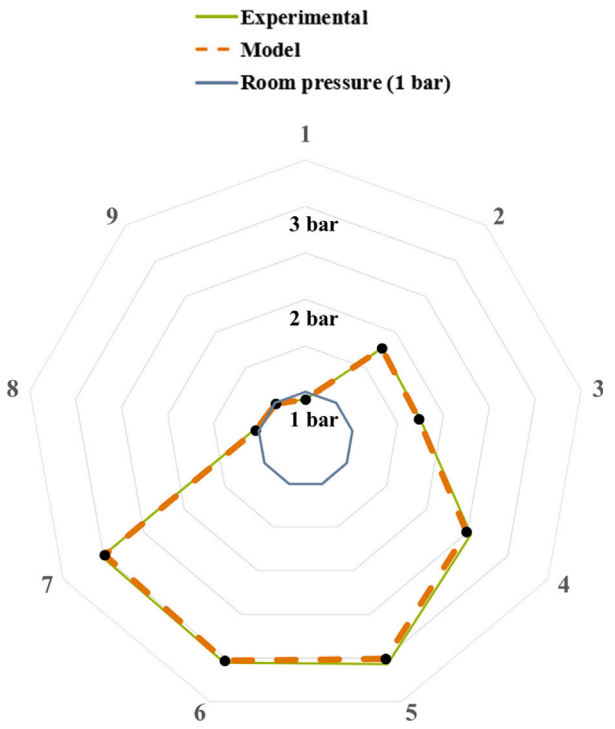


**Fig. 5.** Validation of pressure in the cycle.

ideal pipes (to minimize the impact of the arrangement of the components in the calculations) was used for the exergy analysis. Once the model pipes have been idealized, the components of the cycle are set as real (experimental test proven performance), unavoidable (current technological barrier), and ideal (maximum theoretical efficiency) according to the values from Table 2. The criteria to meet the unavoidable conditions has been developed according to acquirable components. In the case of the turbine, data from Chen and Baines (1994) pointed that efficiencies over 80% could be expected in radial turbines, but in the case of turbochargers, the importance of size and inertia demanded turbines with flow coefficients above the optimum range. Thus, with a commercial turbocharger, the chosen efficiency as unavoidable is taken as representative, without breaking a conservative margin not to obtain unachievable results. Furthermore, results from Serrano et al. (2022) showed the possibility of obtaining higher efficiencies under extremely low-temperature conditions. Therefore, the chosen isentropic efficiency is justified with current turbocharger technology, being coincident with the peak expansion efficiency reported by Wang et al. (2017) in an RBC. In the case of the electric compressors, research on commercially available products has been done using the Rotrex® catalog and other manufacturers. For the size of the facility and the order of MFR employed, peak isentropic efficiencies in these electrically-driven centrifugal compressors are around 80%. In the case of the regenerator, efficiencies around 88 – 90% are easy to find in the market. However, values higher than 92 – 94% demand an overwhelming increase in the element size, though the chosen value of unavoidable efficiency for the regenerator would need one of greater size in comparison with the current one (with a total net volume in both branches of 26 liters, and package dimension volume equivalent to 43 liters).

All of these assumptions provoke a difference between the experimental results and the hereinafter considered as modeled real case. Still, authors consider the components as a proper approach to real conditions since the model has been able to replicate the experimental results.

A comparison between cycles where all of their components are either real, unavoidable, or ideal can be seen in Fig. 6, where the

**Table 2**
RBC components assumptions for the three modeled cases.

| Component | | Real | Unavoidable | Ideal |
|---|---|---|---|---|
| EC1 | $\eta$ | 72% | 80% | 100% |
| IC1 | $\Delta T$ | $8K$ | $2K$ | $0K$ |
| EC2 | $\eta$ | 75% | 80% | 100% |
| TCC | $\eta$ | 63% | 80% | 100% |
| IC2 | $\Delta T$ | $4K$ | $2K$ | $0K$ |
| Reg | $\eta$ | 89% | 94% | 100% |
| Turb | $\eta$ | 61% | 80% | 100% |

different steps are represented with numbers corresponding to the stations of Fig. 3 (the numbers have just been set next to the real cycle points for simplicity). The compression stage from EC1 is represented in 1–2. After that, 2–3 corresponds with the IC1 process. Consequently, 3–4 and 4–5 are the compression steps for the EC2 and the TCC, respectively, with no intermediate cooling. Once again, in 5–6, the air is cooled down with water in the IC2, and 6–7 is defined as the hot side of the regenerator. When the fluid leaves the regenerator at a temperature below 200 K for every case, it enters the turbine, corresponding the 7–8 process to the expansion that takes place in the turbine. The interval 8–9 is the thermal load cooling, which is why point 9 remains equal for each case, its pressure is set as ambient, and the temperature was the objective of 173 K (−100 °C). From that point, the cycle is closed through the process 9–1, representing the cold side of the regenerator. Each cycle has a different MFR, provoking that process 8–9 has different starting points despite having the same thermal load applied. This is illustrated in Eq. (22) where the lower the mass flow, the bigger the temperature leap necessary to dissipate the power in the thermal load.

$$\dot{W} = \dot{m} c_p (T_9 - T_8) \tag{22}$$

Considering that point 9 from Fig. 3 is fixed at a constant temperature and pressure (because of the imposed boundary conditions of −100 °C and ambient pressure), the next point of the cycle, point 1 also from Fig. 3, becomes colder the lower the regenerator efficiency is. Being further to their corresponding point 6, which is set by the cooling water temperature and the IC2 efficiency. Despite starting the compression process 1–2 at a higher temperature, the increase in efficiency for EC1 is so relevant for the cycle performance that the outlet temperature (point 2) is lower the higher the EC1 efficiency is. That also implies that the coolers will work at lower demanding conditions, even if their efficiency would not increase, which is more notable at the IC2 stage (5–6) since point 6 is almost the same for every case. Still, point 5 is lower in temperature the higher the efficiency of the RBC is. Regarding the compression stages 3–4 and 4–5, the impact of the lower efficiency of the TCC in the real RBC is remarkable compared to the efficiency of the EC2 (what is visible with the change in the slope at point 4). Besides, with the efficiency increase in the turbine, the maximum pressure required for achieving the point of dissipating 1.5 kW at −100 °C is reduced. This provokes that the amount of work required of the electric compressors diminishes, reducing cycle energy consumption. This can be well seen between the ideal and the real cases in Fig. 6; meanwhile the 3–4 process is much bigger than 4–5 in terms of temperature leap for the real case, the situation is reversed for the ideal case, increasing the contribution of the TCC and reducing the necessity of power provided by EC2. The efficiency of the turbine, by its part, is a key factor not just for the aforementioned contribution to the TCC power but also because the pressure leap needed in the process of expansion 7–8 is reduced according to the increase of efficiency. This reduction means that lower peak pressures are necessary to achieve the desired purpose of refrigeration. The best proof of this is that the pressure level in the 2–3 process for the real cycle is almost the same as the pressure level 5-6-7 for the ideal cycle, despite starting from a higher temperature in point 1 of the cycle for the ideal process.

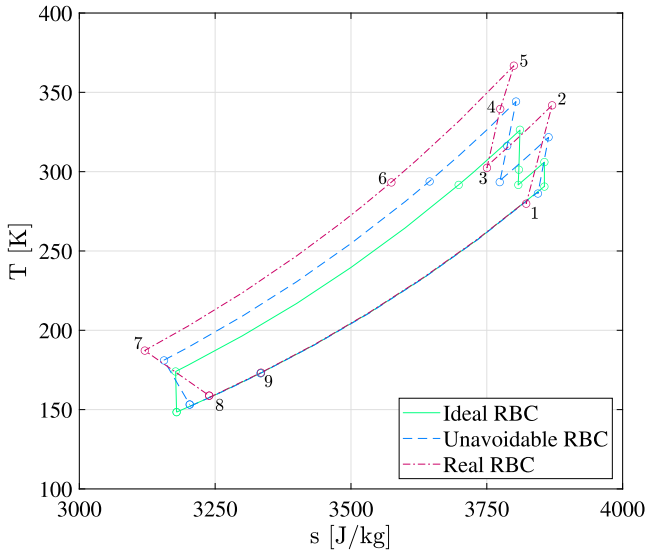


**Fig. 6.** Temperature vs entropy diagram in the RBC for the three modeled cases.

**Table 3**
Thermodynamic properties in each station of the RBC under Real conditions.

| | P [bar] | T [°C] | h [kJ/kg] | s [kJ/kg K] | $e^T$ [kJ/kg] | $e^M$ [kJ/kg] | $\dot{E}$ [kW] |
|---|---|---|---|---|---|---|---|
| 1 | 0.99 | 6.6 | 406.0 | 3.82 | 0.59 | −1.77 | −0.13 |
| 2 | 1.70 | 68.7 | 468.3 | 3.87 | 2.94 | 44.03 | 5.14 |
| 3 | 1.67 | 26.3 | 428.6 | 3.75 | 0.03 | 42.97 | 4.71 |
| 4 | 2.31 | 66.3 | 465.9 | 3.78 | 2.65 | 70.30 | 7.99 |
| 5 | 2.77 | 93.6 | 493.4 | 3.80 | 6.93 | 86.05 | 10.18 |
| 6 | 2.76 | 20.1 | 419.1 | 3.57 | 0.04 | 85.85 | 9.40 |
| 7 | 2.76 | −86.0 | 311.8 | 3.12 | 28.19 | 85.76 | 12.47 |
| 8 | 1.04 | −114.4 | 284.1 | 3.24 | 48.85 | 2.07 | 5.57 |
| 9 | 1.01 | −99.9 | 298.8 | 3.33 | 37.16 | 0.05 | 4.07 |

In Table 3, 4, and 5, thermodynamic properties of the three represented cycles in Fig. 6 are shown numerically. Peak pressure can be quantified here, from the 2.77 bar from the real cycle to the 1.77 bar in the ideal one. Besides, the necessary electric input to the cycle is notably reduced since, in the ideal case, the combined pressure ratio for the two electric compressors is 1.33; meanwhile, in the real case, just the pressure ratio of EC1 is slightly over 1.70. From these results, it can also be pointed the potential improvement in the cycle by minimizing pipe losses. Experimental results from Fig. 5 showed that the maximum pressure in the cycle to achieve the desired refrigeration conditions was 3 bar; however, with the simplifications applied to the modeling of the pipes, the maximum pressure drops to 2.77 bar, with the subsequent electric compressors energy demand reduction. Exergy terms are shown in the last three columns, with the specific exergy divided into thermal and mechanical. Although the specific thermal exergy at point 9 is nearly the same for all of the studied cases (and the mechanical is negligible for being near to ambient reference pressure), it can be seen the exergy varies widely from the 2.55 kW in the ideal case to the 4.07 kW of the real case, this is due to the variation in mass flow ratio in the cycle for the different simulated cases. Besides, in the ideal case, it can be seen that the highest temperature achieved is 54.2 °C, reducing more than five times the specific thermal exergy in the hot part when compared to the real case, implying less cooling power required to the inter-coolers.

Results for the energy analysis of the RBC for the three cases are shown in Table 6, net power of each element in the cycle for the real, unavoidable, and ideal cases alongside with COP obtained as in Eqs. (1) and (2). It is appreciated that the reduction in power provided by the

**Table 4**
Thermodynamic properties in each station of the RBC under Unavoidable conditions.

| | P [bar] | T [°C] | h [kJ/kg] | s [kJ/kg K] | $e^T$ [kJ/kg] | $e^M$ [kJ/kg] | $\dot{E}$ [kW] |
|---|---|---|---|---|---|---|---|
| 1 | 1.00 | 13.0 | 412.4 | 3.84 | 0.25 | −1.46 | −0.10 |
| 2 | 1.40 | 48.6 | 448.1 | 3.86 | 0.89 | 27.78 | 2.27 |
| 3 | 1.39 | 20.3 | 419.6 | 3.77 | 0.04 | 26.90 | 2.13 |
| 4 | 1.72 | 43.1 | 442.5 | 3.79 | 0.53 | 45.24 | 3.62 |
| 5 | 2.19 | 71.0 | 470.6 | 3.80 | 3.26 | 65.78 | 5.46 |
| 6 | 2.18 | 20.6 | 419.8 | 3.65 | 0.03 | 65.59 | 5.19 |
| 7 | 2.18 | −92.1 | 305.9 | 3.16 | 31.99 | 65.51 | 7.71 |
| 8 | 1.04 | −119.9 | 278.5 | 3.20 | 53.96 | 2.06 | 4.43 |
| 9 | 1.01 | −100.3 | 298.4 | 3.33 | 37.48 | −0.43 | 2.93 |

**Table 5**
Thermodynamic properties in each station of the RBC under Ideal conditions.

| | P [bar] | T [°C] | h [kJ/kg] | s [kJ/kg K] | $e^T$ [kJ/kg] | $e^M$ [kJ/kg] | $\dot{E}$ [kW] |
|---|---|---|---|---|---|---|---|
| 1 | 1.01 | 17.4 | 416.8 | 3.86 | 0.10 | −0.53 | −0.03 |
| 2 | 1.21 | 32.9 | 432.3 | 3.86 | 0.10 | 15.04 | 1.05 |
| 3 | 1.21 | 18.5 | 417.9 | 3.81 | 0.07 | 15.04 | 1.04 |
| 4 | 1.33 | 28.1 | 427.5 | 3.81 | 0.02 | 23.49 | 1.62 |
| 5 | 1.77 | 54.2 | 453.7 | 3.82 | 1.35 | 47.56 | 3.38 |
| 6 | 1.77 | 18.5 | 417.7 | 3.70 | 0.07 | 47.56 | 3.29 |
| 7 | 1.77 | −99.1 | 299.1 | 3.18 | 36.76 | 47.56 | 5.82 |
| 8 | 1.01 | −122.5 | 275.9 | 3.20 | 56.49 | −0.53 | 3.86 |
| 9 | 1.01 | −100.2 | 298.5 | 3.33 | 37.40 | −0.53 | 2.55 |

electric compressors is much higher than the one from the turbine power. Comparing the real and the ideal case in Table 6, it can be seen how the reduction in power is between 6 and 7 times for the electric compressors. Meanwhile, the turbine power is lowered by less than half between the same cases. This reduction comes from the increase in efficiency and the decrease in mass flow ratio for the ideal RBC, demanding less work for the compressors. For the coolers, the heat dissipated is also reduced, mainly due to the fact that the compressor outlet temperature becomes lower, as previously stated. Regarding the regenerator, the reduction in the power of its branches is not as big as in the other components because the temperature leap is similar, and the decrease of heat interchanged between its branches is mostly due to the reduction of mass flow, which varies between the real and the ideal case about a 35%. The cycle COP for the real case is 0.14, showing that the technical limitation is about 0.33 and there is a margin to improve the efficiency in the cycle for the desired application. However, with ideal components, the ceiling of the COP is much higher, reaching theoretically 0.87. According to FOM values, the COP that the facility reaches rises from 0.11 in the real case to 0.7 for the ideal case, being the limit of this figure 1. It is worth mentioning that these COP values are valid for the cycle display shown in Fig. 3 and the temperature and thermal load requirements of this application. The lower maximum pressure requirements imply that three serial compression stages could not be needed.

The Grassmann diagram applied to the RBC in real conditions allows an understanding of the flow of exergy between components (see Fig. 7). Both electric compressors receive their fuel exergy from external sources, with EC1 getting nearly as double as EC2. The turbine available exergy product (5.4 kW) is divided into 1.5 kW for refrigeration capacity (applied to the thermal load in the CC) and recirculations of exergy, divided in 0.7 kW to the regenerator ($\dot{E}^T$) and 3.2 kW to the turbocharger compressor ($\dot{E}^M$). It can also be seen how the destructed exergy of the turbine is the greatest of each element by far and that EC2, TCC, IC2, and the regenerator have a similar amount of destructed exergy. Both inter-coolers have a slight contribution to fuel exergy due to the negative value of their product exergy. This negative value comes from the chosen reference temperature $T_0 = 25$ °C. Since the inlet water temperature is 18 °C and its outlet temperature is closer to the reference temperature, the amount of exergy is decreased according to Eq. (6).

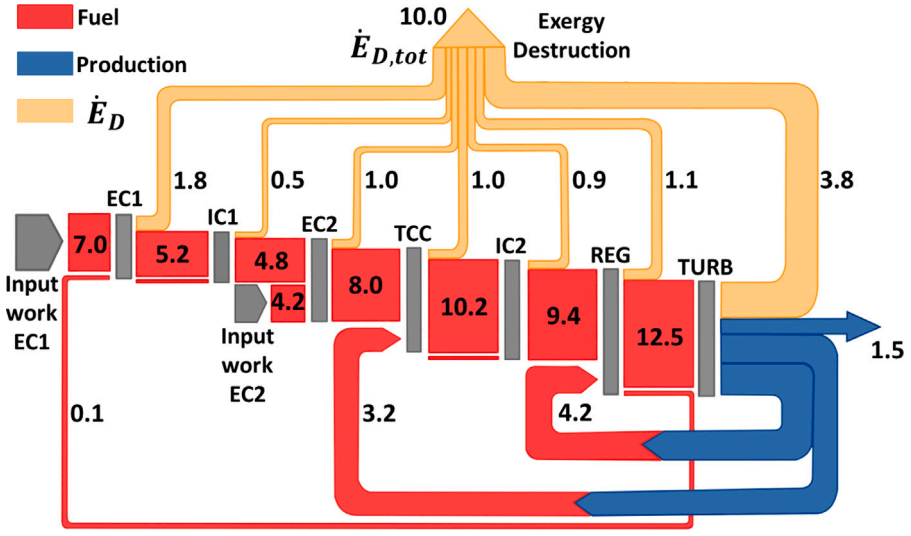


**Fig. 7.** Grassmann diagram for the RBC under Real conditions.

**Table 6**
Power and efficiency in the components of the RBC according to the modeled cases.

| | Real | Unavoidable | Ideal |
|---|---|---|---|
| $\dot{W}_{EC1}$ [kW] | 7.03 | 2.92 | 1.14 |
| $\dot{W}_{EC2}$ [kW] | 4.23 | 1.85 | 0.61 |
| $\dot{W}_{TCC}$ [kW] | 3.17 | 2.24 | 1.76 |
| $\dot{W}_{Turb}$ [kW] | 3.20 | 2.26 | 1.77 |
| $\dot{Q}_{IC1}$ [kW] | 4.33 | 2.25 | 0.99 |
| $\dot{Q}_{IC2}$ [kW] | 8.13 | 4.02 | 2.52 |
| $\dot{Q}_{Reg,HS}$ [kW] | 11.84 | 9.08 | 8.24 |
| $\dot{Q}_{Reg,CS}$ [kW] | 11.88 | 9.12 | 8.27 |
| $COP_{actual}$ [-] | 0.142 | 0.330 | 0.868 |
| $COP_{ideal}$ [-] | 1.30 | 1.25 | 1.24 |
| FOM [–] | 0.11 | 0.26 | 0.70 |

**Table 7**
Exergy analysis for RBC under Real conditions.

| | $\dot{E}_F$ [kW] | $\dot{E}_P$ [kW] | $\dot{E}_D$ [kW] | $\epsilon$ [%] | $Y_k$ [%] | $Y_k^*$ [%] |
|---|---|---|---|---|---|---|
| EC1 | 7.03 | 5.27 | 1.76 | 75 | 25 | 18 |
| IC1 | 0.43 | −0.08 | 0.52 | −19 | 119 | 5 |
| EC2 | 4.23 | 3.28 | 0.96 | 77 | 23 | 10 |
| TCC | 3.17 | 2.19 | 0.97 | 69 | 31 | 10 |
| IC2 | 0.78 | −0.13 | 0.90 | −16 | 116 | 9 |
| Reg | 4.20 | 3.07 | 1.13 | 73 | 27 | 11 |
| Turb | 9.16 | 5.40 | 3.76 | 59 | 41 | 38 |
| RBC | 11.26 | 1.50 | 10.01 | 13 | 89 | 100 |

Conventional exergy analysis results are shown in Table 7, 8, and 9. The analysis for each cycle element has been done as shown in Table 1. The fuel in the cycle is considered to be the sum of EC1 and EC2. Meanwhile, the product of the cycle is the power dissipated in the climatic chamber. In Table 7, it can be seen how the biggest exergy destruction comes from the turbine side, meaning more than one-third of the total exergy destroyed in the cycle, followed by the EC1 and the regenerator, having the two of them combined around 3 kW of destructed exergy. These three components are the ones that should be first attempted to be improved. The turbine has the lowest exergy efficiency (apart from the coolers), with the highest exergy destruction ratio contribution ($Y_k^*$). A similar exergy destruction ratio distribution

**Table 8**
Exergy analysis for RBC under Unavoidable conditions.

| | $\dot{E}_F$ [kW] | $\dot{E}_P$ [kW] | $\dot{E}_D$ [kW] | $\epsilon$ [%] | $Y_k$ [%] | $Y_k^*$ [%] |
|---|---|---|---|---|---|---|
| EC1 | 2.92 | 2.36 | 0.56 | 81 | 19 | 16 |
| IC1 | 0.14 | −0.05 | 0.18 | −34 | 134 | 5 |
| EC2 | 1.85 | 1.49 | 0.36 | 81 | 19 | 10 |
| TCC | 2.24 | 1.84 | 0.40 | 82 | 18 | 12 |
| IC2 | 0.27 | −0.08 | 0.35 | −28 | 128 | 10 |
| Reg | 3.02 | 2.52 | 0.51 | 83 | 17 | 15 |
| Turb | 5.02 | 3.95 | 1.06 | 79 | 21 | 31 |
| RBC | 4.76 | 1.50 | 3.41 | 31 | 72 | 100 |

for each element appears in Table 8 for the unavoidable case, but with a significant decrease in the total exergy destruction of the RBC from the 10 kW of the real case, to the 3.4 kW of the unavoidable conditions. Once the ideal conditions are applied, the whole exergy destruction becomes the 14% of the fuel exergy (0.37 kW). As an additional visualization to the exergy destruction, Fig. 8 shows the share of each element to the total $\dot{E}_{D,k}$. The distribution in the chart shows that the real and the unavoidable cycles are equivalent in terms of the contribution of each element. Meanwhile, the heat exchanger components, represented by coolers and the regenerator, are the main contributors to the exergy destruction of the ideal cycle. However, the total values of destructed exergy are small. The RBC exergy efficiency starts at 13% in the real case and increases to 31% and 86% for the unavoidable and ideal cases, respectively. To sum up, the conventional exergy analysis reveals the turbine to be the key element in improving RBC performance, followed by EC1 and the regenerator. Furthermore, the advanced exergy analysis is necessary to tell apart the influence of each element on others.

One cycle per element in the RBC has been calculated for the advanced exergy analysis. Results for the endogenous/exogenous, avoidable/unavoidable, and combined approaches are shown in Table 10, where the different parameters for each element have been calculated as shown in Eqs. (13)–(21). Each hybrid cycle uses real conditions for the correspondent element and ideal conditions for every other element according to the data shown in Table 2. Meanwhile, for the

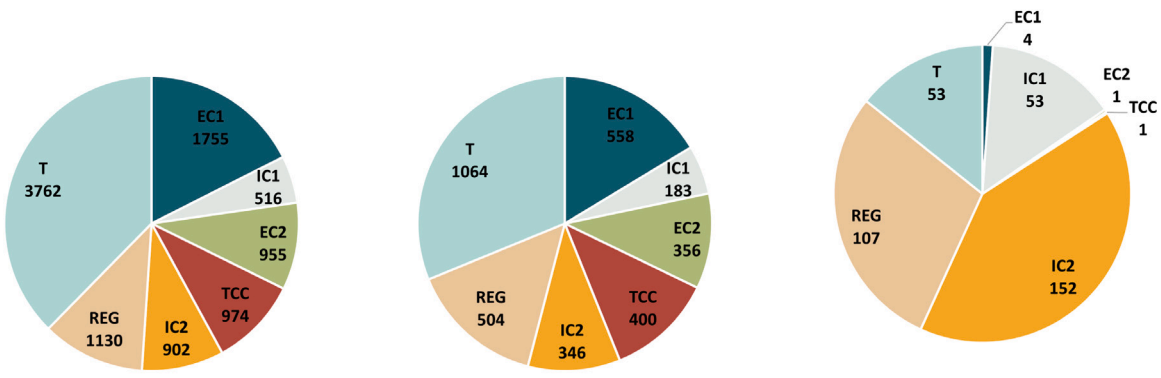


(a) Real cycle (b) Unavoidable cycle (c) Ideal cycle

**Fig. 8.** Destruction of exergy in RBC. Data in W.

**Table 9**
Exergy analysis for RBC under Ideal conditions.

| | $\dot{E}_F$ [kW] | $\dot{E}_P$ [kW] | $\dot{E}_D$ [kW] | $\epsilon$ [%] | $Y_k$ [%] | $Y_k^*$ [%] |
|---|---|---|---|---|---|---|
| EC1 | 1.14 | 1.14 | 0.00 | 99.6 | 0.4 | 1.1 |
| IC1 | 0.03 | −0.02 | 0.05 | −66.4 | 166.4 | 14.3 |
| EC2 | 0.61 | 0.61 | 0.00 | 99.8 | 0.2 | 0.3 |
| TCC | 1.76 | 1.76 | 0.00 | 100 | 0.0 | 0.2 |
| IC2 | 0.10 | −0.05 | 0.15 | −50.5 | 150.5 | 40.9 |
| Reg | 2.63 | 2.53 | 0.11 | 95.9 | 4.1 | 28.9 |
| Turb | 3.12 | 3.07 | 0.05 | 98.3 | 1.7 | 14.3 |
| RBC | 1.75 | 1.50 | 0.37 | 85.8 | 14.2 | 100 |

unavoidable condition cycle, all of the components are set with the defined unavoidable efficiencies.

In Table 10 can be seen how the split between endogenous and exogenous exergy varies a lot between different components. For the coolers and the electric compressors, the majority of the destroyed exergy is exogenous, meaning that their contribution to the cycle could be improved by improving other components or rearranging their position, reducing their destruction rate and improving the cycle efficiency. The opposite effect can be clearly seen in the turbine. Most of its exergy destruction is endogenous, meaning an increase in isentropic efficiency in the turbine could enhance RBC. The boundaries for improving the whole system can be seen by checking the avoidable and unavoidable columns. Hence, the 45% of the exergy destruction rate is avoidable according to the analysis, half of that being attributed to the turbine. The other components with more margin for avoidable exergy destruction rate are the EC1, TCC, and regenerator. The interactions between different components can be either positive or negative, which is the reason why some ratios of destroyed exergy can be positive or negative. According to the analysis, $\dot{E}_{D,IC2}^{EN,AV}$ and $\dot{E}_{D,EC2}^{EX,AV}$ are negative with a small value. The case of the IC2, being endogenous exergy destruction, can be attributed to the leap between the water line temperature 18.5 °C and the reference temperature of the analysis $T_0$ = 25 °C. When the water is heated in the inter-cooler, its outlet specific exergy can be diminished if the outlet temperature is closer to the reference one, $T_0$. Consequently, the increase in thermal efficiency in the inter-coolers is a trade-off in terms of exergy depending on the temperature of the water line with respect to the one taken as a reference for the calculations. Notwithstanding, its effect is quite low compared to the total avoidable exergy destruction rate. In the case of EC2, the negative term comes from an exogenous contribution. This is also an effect derived from the water line temperature since it directly affects the EC2 inlet air temperature, being IC1 placed right before it. Again, the contribution is minimal and can be ignored.

The combined approach is useful to know the real potential for improvement of each element since an increase in the efficiency of a particular element can only reduce the endogenous part of its avoidable exergy destruction rate. Thus, the $\dot{E}_D^{EN,AV}$ is the key value for improving cycle performance. In this case, the 33% of the RBC exergy destruction rate can be avoided, where 2.3 of the 3.3 kW avoidable corresponds to the turbine. Meanwhile, its $\dot{E}_D^{EX,AV}$ part is negligible so that no other element improvement will affect turbine performance, and the most important cycle efficiency enhancement is directly increasing turbine isentropic efficiency. The contribution of other components is one order of magnitude below the capacity for improvement of the turbine. The three compressors and the regenerator can directly reduce the exergy destruction rate between 0.24 and 0.31 kW. The components which are most benefited from the improvement of others are the two inter-coolers, since the 95% in the IC1 and the 120% (due to negative value in $\dot{E}_{D,IC2}^{EN,AV}$) in the IC2 of their avoidable exergy destruction rate is exogenous, mainly due to the reduce in outlet compressor temperatures when the isentropic efficiencies of the compressors increase.

Another visualization for the data from Table 10 can be seen in the **APPENDIX** where Figs. 10–16 show the approaches endogenous/exogenous, avoidable/unavoidable and both combined for each element in the RBC, this is, EC1, IC1, EC2, TCC, IC2, regenerator, and turbine, reinforcing the analysis extracted from the table, the turbine is by far the element in which there is more margin for improvement attending the percentage of $\dot{E}_D^{EN,AV}$, followed by the TCC that is the only other element having its avoidable endogenous exergy surpassing one-quarter of its total exergy destruction rate. In both of the inter-coolers, their avoidable exogenous exergy is around one-third of their overall exergy destruction rate. The two electric compressors alongside IC1 are the components with the highest proportion of unavoidable exogenous exergy destruction rate, being around half of its total $\dot{E}_D$. The regenerator, by its part, is the component with the highest proportion of unavoidable endogenous exergy destruction rate, meaning that even reaching its peak available efficiency, most of the endogenous exergy destruction cannot be overcome.

The importance of the turbine isentropic efficiency can be emphasized by comparing the different COP values obtained for the different cycles studied. In Table 6, there were data for the real, unavoidable, and ideal cycles, but the hybrid cycles (where an element is kept real and the others are set as ideal) are not represented there. In Fig. 9, the former three cycles and the seven hybrid cycles (one per cycle element) COP values are shown. Each point represents the COP of the cycle of its x-coordinate. From the hybrid cycles, it can be seen how the improvement in the coolers can be prejudicial for the cycle COP. The change they provoke can be considered equivalent to varying

**Table 10**
Advanced exergy analysis.

| | $\dot{E}_D$ [kW] | $\dot{E}_D^{EN}$ [kW] | $\dot{E}_D^{EX}$ [kW] | $\dot{E}_D^{AV}$ [kW] | $\dot{E}_D^{UN}$ [kW] | $\dot{E}_D^{EN,AV}$ [kW] | $\dot{E}_D^{EN,UN}$ [kW] | $\dot{E}_D^{EX,AV}$ [kW] | $\dot{E}_D^{EX,UN}$ [kW] |
|---|---|---|---|---|---|---|---|---|---|
| EC1 | 1.75 | 0.55 | 1.20 | 0.51 | 1.25 | 0.28 | 0.27 | 0.23 | 0.98 |
| IC1 | 0.52 | 0.08 | 0.44 | 0.19 | 0.32 | 0.01 | 0.08 | 0.19 | 0.25 |
| EC2 | 0.96 | 0.39 | 0.56 | 0.17 | 0.79 | 0.24 | 0.15 | −0.07 | 0.63 |
| TCC | 0.97 | 0.58 | 0.40 | 0.50 | 0.48 | 0.31 | 0.26 | 0.18 | 0.21 |
| IC2 | 0.90 | 0.15 | 0.75 | 0.33 | 0.57 | −0.07 | 0.22 | 0.40 | 0.35 |
| Reg | 1.13 | 0.73 | 0.40 | 0.52 | 0.61 | 0.26 | 0.48 | 0.26 | 0.14 |
| Turb | 3.76 | 3.13 | 0.63 | 2.31 | 1.45 | 2.30 | 0.83 | 0.01 | 0.62 |
| RBC | 10.01 | 5.62 | 4.38 | 4.52 | 5.47 | 3.32 | 2.29 | 1.20 | 3.18 |

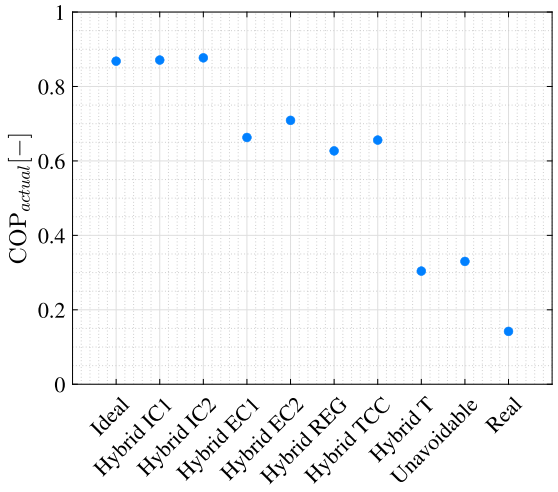


**Fig. 9.** COP value for every cycle.

cooling water temperatures, which would be another parameter to study. The three compressors and the regenerator hybrid cycles COP range lies between 0.6 and 0.7. Their peak is the hybrid EC2 cycle since its compression ratio is the lowest and its real efficiency the highest. This proves that improving the other compressors has a greater effect in terms of cycle efficiency. Finally, a clue point to understand the importance of the turbine is that its hybrid cycle is the only one that offers a COP below the unavoidable cycle. This means that increasing the isentropic efficiency turbine from the real to the technological limit (set as 80% at Table 2) is more beneficial than considering that any other component in the cycle turns ideal while the turbine is not modified at all.

## 5. Conclusions

This paper evaluates the performance of an electric RBC designed for diverse cryogenic uses. The novelty lies in the use of automotive components and air as the sole working fluid, avoiding high GWP refrigerants. Through analyzing the exergy destruction rate and simulating the RBC thermal and fluid dynamics, critical points of the cycle were evaluated. Key conclusions are highlighted in the present section.

- Based on the conventional exergy analysis, the turbine represents the 38% of the total exergy destruction rate in the cycle. Consequently, it is the first element that should be improved, followed by the EC1 (which takes the greatest part in the compression work). Meanwhile, the regenerator, the EC2, the TCC, and the IC2 have a similar contribution of around 10% each.
- Advanced exergy analysis reveals that the endogenous exergy of the turbine greatly surpasses its exogenous part. Therefore, enhancing turbine efficiency can significantly decrease exergy destruction. About 61% (2.3 kW) of its endogenous exergy can be avoided. EC1 has the highest exogenous exergy, influenced by turbine performance that sets the required mass flow ratio. In a combined approach, 78% of the exogenous exergy of EC1 is inevitable, indicating most losses will persist even with other component improvements. Looking at the avoidable exogenous exergy destruction, IC2 and the regenerator could see the most benefits, with potential savings of 44% and 23% of their total exergy destruction, respectively.
- Current COP obtained in the facility for the boundary conditions applied is around 0.13 (slightly increased in the real cycle analyzed because of the assumptions taken for the calculations). This value can be increased by modifying components for other commercially available up to 0.33, according to the results obtained in this paper.
- When only the turbine is non-ideal (and every other element is), the cycle performance is worse than when all elements are at their technological limit. Thus, this reinforces the idea of the turbine being the key element in the cycle. A turbine achieving peak efficiency of 80% would make the cycle COP competitive with other gas technologies like $CO_2$ or ammonia.

## Declaration of competing interest

The authors declare that they have no known competing financial interests or personal relationships that could have appeared to influence the work reported in this paper.

## Acknowledgments

The authors want to acknowledge the institution “Conselleria de Innovaciòn, Universidades, Ciencia *y* Sociedad Digital de la Generalitat Valenciana” and its grant program “Subvenciones para la contrataciòn de personal investigador de caràcter predoctoral” for doctoral studies (CIACIF/2021/404) funded by The European Union; also the institution “Vicerrectorado de Investigaciòn de la Universitat Politècnica de València” for the funding provided by the research project (PAID-11-22)”. This work has been partially supported by Grant PID2021-123351OB-I00 funded by MCIN/AEI/ 10.13039/501100011033 and, as appropriate, by “ERDF A way of making Europe”.

## Appendix

See Figs. 10–16.

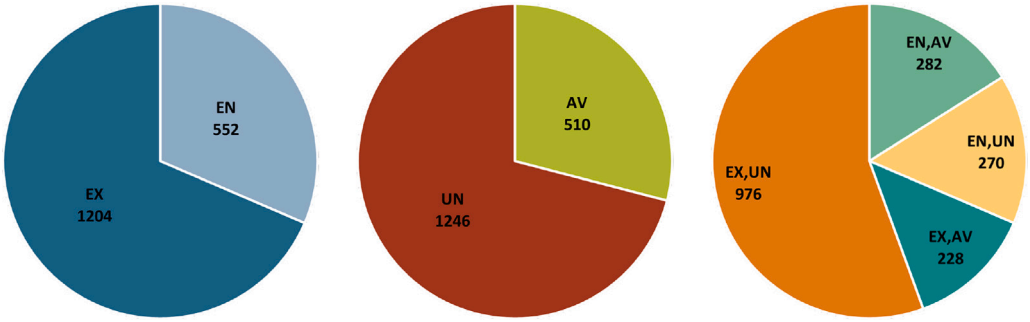


**Fig. 10.** Advanced exergy balance for the EC1. Exergy destruction rate. Data in W.

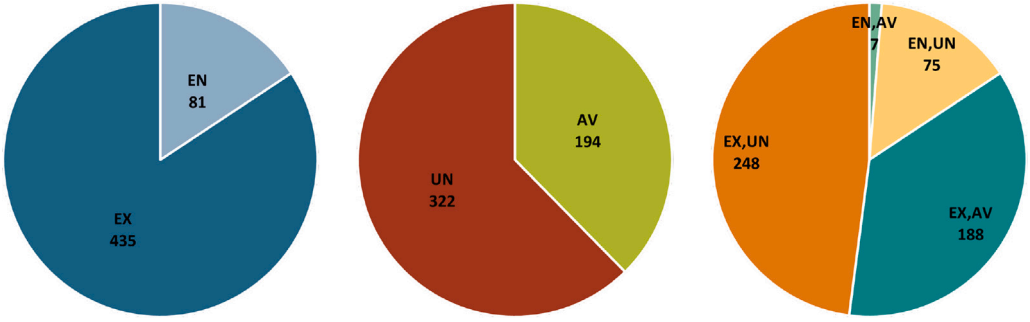


**Fig. 11.** Advanced exergy balance for the IC1. Exergy destruction rate. Data in W.

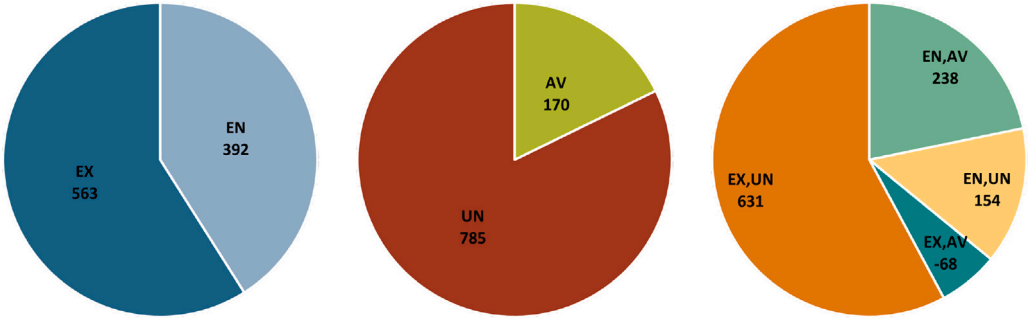


**Fig. 12.** Advanced exergy balance for the EC2. Exergy destruction rate. Data in W.

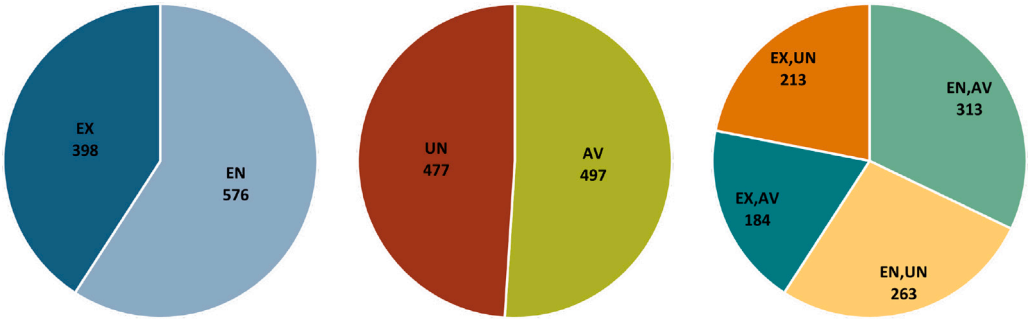


**Fig. 13.** Advanced exergy balance for the TCC. Exergy destruction rate. Data in W.

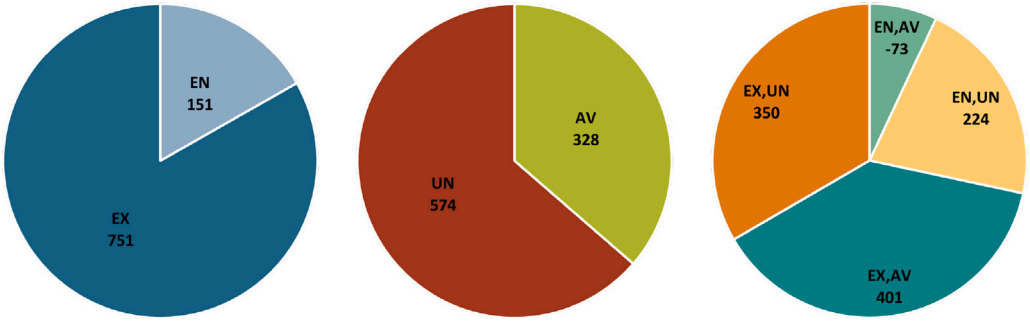


**Fig. 14.** Advanced exergy balance for the IC2. Exergy destruction rate. Data in W.

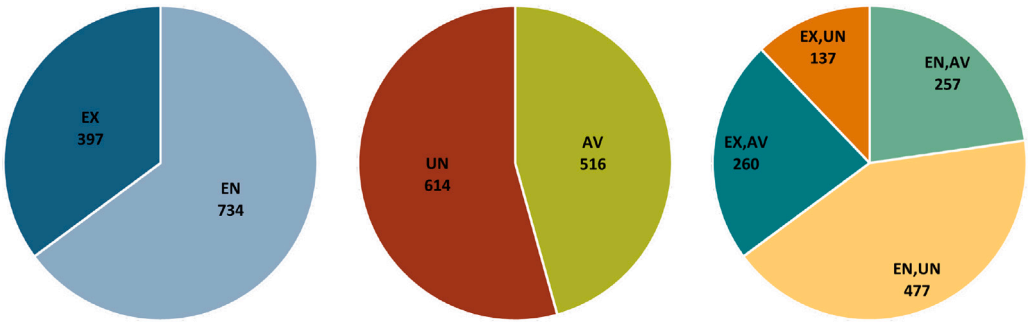


**Fig. 15.** Advanced exergy balance for the regenerator. Exergy destruction rate. Data in W.

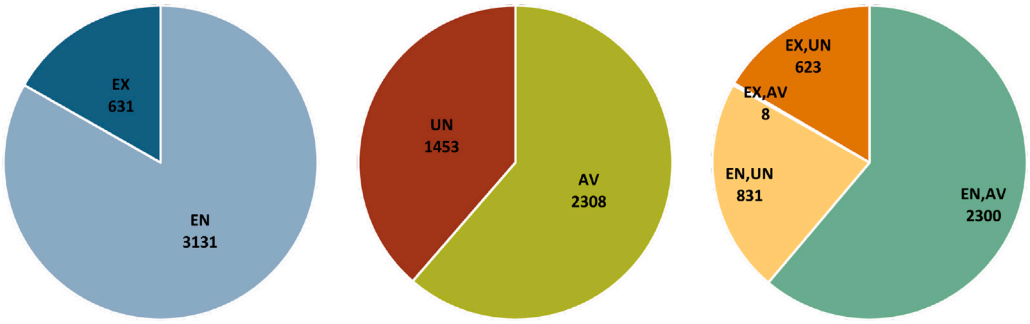


**Fig. 16.** Advanced exergy balance for the turbine. Exergy destruction rate. Data in W.

## References


Asgari, S., Noorpoor, A., Boyaghchi, F.A., 2017. Parametric assessment and multi-objective optimization of an internal auto-cascade refrigeration cycle based on advanced exergy and exergoeconomic concepts. Energy 125, 576–590.

Bakshi, B.R., Gutowski, T.G., Sekulić, D.P., 2011. Thermodynamics and the Destruction of Resources. Cambridge University Press, pp. 377–401.

Bell, I.H., Wronski, J., Quoilin, S., Lemort, V., 2014. Pure and pseudo-pure fluid thermophysical property evaluation and the open-source thermophysical property library CoolProp. Ind. Eng. Chem. Res. 53 (6), 2498–2508. http://dx.doi.org/10.1021/ie4033999, arXiv:http://pubs.acs.org/doi/pdf/10.1021/ie4033999.

Biglia, A., Comba, L., Fabrizio, E., Gay, P., Mannini, A., Mussinatto, A., Aimonino, D.R., 2017. Reversed brayton cycle for food freezing at very low temperatures: Energy performance and optimisation. Int. J. Refrig. 81, 82–95.

Biglia, A., Messina, C., Comba, L., Aimonino, D.R., Gay, P., Brugiapaglia, A., 2022. Quick-freezing based on a nitrogen reversed brayton cryocooler prototype: Effects on the physicochemical characteristics of beef longissimus thoracis muscle. Innov. Food Sci. Emerg. Technol. 82, 103208.

Chen, H., Baines, N., 1994. The aerodynamic loading of radial and mixed-flow turbines. Int. J. Mech. Sci. 36 (1), 63–79.

Chen, J., Havtun, H., Palm, B., 2015. Conventional and advanced exergy analysis of an ejector refrigeration system. Appl. Energy 144, 139–151.

Dhillon, A.K., Ghosh, P., 2021. Exergetic analysis of reverse brayton cryocooler with different turbine arrangements for HTS power cables. Cryogenics 115, 103262.

Dugue, B., Bernard, J.-P., Bouzigon, R., Nardi, M., Douzi, W., Feirreira, J., Guilpart, J., Lombardi, G., Miller, E., Tiemessen, I., 2020. Whole body cryotherapy / cryostimulation. 39th informatory note on refrigeration technologies. Int. J. Refrig. http://dx.doi.org/10.18462/iif.NItec39.09.2020.

Dupont, J.-L., Domanski, P., Lebrun, P., Ziegler, F., 2019. The role of refrigeration in the global economy. 38th informatory note on refrigeration technologies. Int. J. Refrig. http://dx.doi.org/10.18462/iif.NItec38.06.2019.

Galindo, J., Dolz, V., Pla, B., Ponce-Mora, A., 2020. Advanced exergy analysis of a jet ejector refrigeration cycle used to cool down the intake air in an internal combustion engine. Int. J. Exergy 32 (4), 388–411.

Galindo, J., Ruiz, S., Dolz, V., Royo-Pascual, L., 2016. Advanced exergy analysis for a bottoming organic rankine cycle coupled to an internal combustion engine. Energy Convers. Manage. 126, 217–227.

Höglund-Isaksson, L., Purohit, P., Amann, M., Bertok, I., Rafaj, P., Schöpp, W., Borken-Kleefeld, J., 2017. Cost estimates of the Kigali amendment to phase-down hydrofluorocarbons. Environ. Sci. Policy 75, 138–147.

Hu, H., Jiang, Y., Guo, C., Liang, S., 2020. Thermodynamic and exergy analysis of a S-CO2 Brayton cycle with various of cooling modes. Energy Convers. Manage. 220, 113110.

Huang, R., Hu, B., Wang, R., Eikevik, T.M., Ge, T., 2022. Thermodynamic and economic analysis of two-stage CO2 heat pump with reverse brayton cycle. Int. J. Refrig. 143, 157–165.

Khalilzadeh, S., Esfandiari, G., Arand, H.J., Adeli, M.M., 2023. Integration of different organic Rankine and Kalina cycles with compressed refrigeration cycle to reduce the power consumption: a comparative study. Int. J. Refrig.

Lu, J., Xia, Y., Cheng, Q., 2023. Improvement of Brayton refrigeration air cycle for electroplating wastewater treatment. Int. J. Refrig. 155, 219–232.

Martin, J., Arnau, F., Piqueras, P., Auñon, A., 2018. Development of an integrated virtual engine model to simulate new standard testing cycles. Tech. Rep., SAE Technical Paper.

Morosuk, T., Tsatsaronis, G., Schult, M., 2013. Conventional and advanced exergetic analyses: theory and application. Arab. J. Sci. Eng. 38, 395–404.

Pambudi, N.A., Sarifudin, A., Gandidi, I.M., Romadhon, R., 2022. Vaccine cold chain management and cold storage technology to address the challenges of vaccination programs. Energy Rep. 8, 955–972.

Petrakopoulou, F., Boyano, A., Cabrera, M., Tsatsaronis, G., 2011. Exergoeconomic and exergoenvironmental analyses of a combined cycle power plant with chemical looping technology. Int. J. Greenhouse Gas Control 5 (3), 475–482.

Qin, Y., Li, N., Zhang, H., Liu, B., 2021. Energy and exergy performance evaluation of a three-stage auto-cascade refrigeration system using low-GWP alternative refrigerants. Int. J. Refrig. 126, 66–75.

Serrano, J.R., Arnau, F.J., García-Cuevas, L.M., Dombrovsky, A., Tartoussi, H., 2016. Development and validation of a radial turbine efficiency and mass flow model at design and off-design conditions. Energy Convers. Manage. 128, 281–293.

Serrano, J.R., Arnau, F.J., García-Cuevas, L.M., Inhestern, L.B., 2019a. An innovative losses model for efficiency map fitting of vaneless and variable vaned radial turbines extrapolating towards extreme off-design conditions. Energy 180, 626–639.

Serrano, J.R., Dolz, V., Ponce-Mora, A., López-Carrillo, J.A., 2022. Experimental assessment of a reverse brayton cycle based on automotive turbochargers and E-chargers for cryogenic applications. J. Eng. Gas Turbines Power 145 (2), http://dx.doi.org/10.1115/1.4055580, 021029. arXiv:https://asmedigitalcollection.asme.org/gasturbinespower/article-pdf/145/2/021029/6960717/gtp_145_02_021029.pdf.

Serrano, J.R., García-Cuevas, L.M., Samala, V., López-Carrillo, J.A., Mai, H., 2021. Boosting the capabilities of gas stand data acquisition and control systems by using a digital twin based on a holistic turbocharger model. In: Internal Combustion Engine Division Fall Technical Conference, Vol. 85512. American Society of Mechanical Engineers, V001T07A002.

Serrano, J.R., Navarro, R., García-Cuevas, L.M., Inhestern, L.B., 2019b. Contribution to tip leakage loss modeling in radial turbines based on 3D flow analysis and 1D characterization. Int. J. Heat Fluid Flow 78, 108423.

Shuailing, L., Guoyuan, M., Shuxue, X., Yuexuan, G., Xiaoya, J., Guoqiang, W., 2022. A review of reverse brayton air cycle refrigerators. Int. J. Refrig.

Spence, S.W., Doran, W.J., Artt, D.W., 2004. Design, construction and testing of an air-cycle refrigeration system for road transport. Int. J. Refrig. 27 (5), 503–510.

Spence, S.W., Doran, W.J., Artt, D.W., McCullough, G., 2005. Performance analysis of a feasible air-cycle refrigeration system for road transport. Int. J. Refrig. 28 (3), 381–388.

Sun, D., Sun, S., Song, Q., Wang, D., Wang, Y., Guo, S., 2023. Energy, exergy, economic and environmental (4E) analysis of two-stage cascade, Linder-Hampson and reverse Brayton systems in the temperature range from- 120°C to- 60° C. Energy 283, 129178.

Timmerhaus, K.D., Flynn, T.M., 2013. Cryogenic Process Engineering. Springer Science & Business Media, pp. 104–107.

United Nations Environment Program, 2023. Amendment To the Montreal Protocol on Substances that Deplete the Ozone Layer. Chapter XXVII. Section 2f. United Nations.

Wang, H., Chen, G., Dong, X., Zhao, Y., Guo, H., Gong, M., 2017. Performance comparison of single-stage mixed-refrigerant Joule–Thomson cycle and pure-gas reverse Brayton cycle at fixed-temperatures from 80 to 180 K. Int. J. Refrig. 80, 77–91.

Wang, L., Li, H., Zhou, J., 2023. Thermodynamic investigation of a centrifugal reverse Brayton cycle for refrigeration in air conditioning filed. Int. J. Refrig.

World Health Organization, et al., 2021. COVID-19 Vaccination: Supply and Logistics Guidance: Interim Guidance, 12 February 2021. Tech. Rep., World Health Organization.

Yana Motta, S., Domanski, P., 2022. Low-GWP refrigerants status and outlook. In: IIR Informatory Note - TBD, Tennessee, United States of America. Oak Ridge National Lab.(ORNL), Oak Ridge, TN (United States).

Yang, X., Chen, L., Wang, Z., Chen, S., Hou, Y., 2023. Study on the coupled characteristics of high-speed centrifugal compressor and turboexpander of a reverse Brayton air refrigerator. Int. J. Refrig. 147, 20–28.